

Risk Assessment of Scramjet Unstart Using Adjoint-Based Sampling Methods

Qiqi Wang*

Massachusetts Institute of Technology, Cambridge, Massachusetts 02139

and

Karthik Duraisamy,[†] Juan J. Alonso,[‡] and Gianluca Iaccarino[§]

Stanford University, Stanford, California 94305

DOI: 10.2514/1.J051264

In this paper, we demonstrate an adjoint-based approach for accelerating Monte Carlo estimations of risk, and we apply it to approximate the unstart probability of a supersonic combustion ramjet (scramjet) engine under changes in uncertain operating conditions characterized by both Gaussian and non-Gaussian distributions. The adjoint equation is formulated with respect to an objective function that has been experimentally shown to be indicative of unstart, and it is used to build a linear surrogate. This surrogate is, in turn, used to divide the uncertain input parameters into three different strata corresponding to safe operation of the engine, uncertain operation, and unstart. The probability of unstart within these strata is very different and, as a result, stratified sampling significantly reduces the variance of the estimator. The efficiency of the stratified sampling procedure is further improved by optimally allocating the number of solution evaluations within each stratum. Using this technique, the estimations from straightforward use of the Monte Carlo method were demonstrated to be accelerated by a factor of more than five.

Nomenclature

\mathcal{C}	= critical value of output functional
C_c	= flame shape parameter 1
D_c	= flame shape parameter 2
\mathbb{E}	= expectation
f_{st}	= stoichiometric fuel/air ratio
H_f	= fuel heating value, MJ/kg
\mathcal{J}	= output functional
$\tilde{\mathcal{J}}$	= surrogate approximation of output functional
K_c	= fraction of completed combustion
L_C	= combustor length, m
m_{air}	= mass flow of air, kg/s
M_I	= Mach number after cowl shock (combustor inlet)
M_1	= Mach number after nose shock
M_∞	= freestream Mach number
\mathbb{P}	= probability
p	= pressure, Pa
p_I	= combustor inlet pressure, Pa
p_1	= pressure after nose shock, Pa
p_∞	= freestream pressure, Pa
Q	= heat release, J/s
R	= governing equation of flowfield
R_H	= discretized governing equation
U_H	= flow variables

Presented as Paper 2010-2921 at the AIAA Non-Deterministic Approaches (NDA) Conference, Orlando, FL, 12–15 April 2010; received 15 March 2011; revision received 2 August 2011; accepted for publication 13 September 2011. Copyright © 2011 by the American Institute of Aeronautics and Astronautics, Inc. All rights reserved. Copies of this paper may be made for personal or internal use, on condition that the copier pay the \$10.00 per-copy fee to the Copyright Clearance Center, Inc., 222 Rosewood Drive, Danvers, MA 01923; include the code 0001-1452/12 and \$10.00 in correspondence with the CCC.

*Assistant Professor, Aeronautics and Astronautics, 77 Massachusetts Avenue. Member AIAA (Corresponding Author).

[†]Assistant Professor, Aeronautics and Astronautics, 488 Escondido Mall. Member AIAA.

[‡]Associate Professor, Aeronautics and Astronautics, 488 Escondido Mall. Member AIAA.

[§]Assistant Professor, Mechanical Engineering, 488 Escondido Mall. Member AIAA.

U_H	= numerical solution of flow variables
Var	= variance
w	= collection of all uncertain parameters
w_0	= mean (or nominal) value of uncertain parameters
X_c	= combustion ignition position, m
Φ	= adjoint solution (Lagrange multiplier)
α	= angle of attack
β_1	= angle of nose shock
β_2	= angle of cowl shock
θ_N	= angle of nose wedge
ρ_I	= combustor inlet density, kg/m ³
ρ_1	= density after nose shock, kg/m ³
ρ_∞	= freestream density, kg/m ³
ϕ	= equivalence ratio
Ω	= physical domain of interest
Ω_H	= computational mesh

I. Introduction

NASA'S X-43 hypersonic vehicle [1] holds the flight speed record among airbreathing propulsion systems, having reached a self-sustained speed of Mach 10 for approximately 10 s in 2004. The X-43 was powered by a supersonic combustion ramjet (scramjet) engine, in which air at supersonic speeds is mixed with hydrogen in the combustion chamber. The resulting ignition and expulsion of the high-velocity gas mixture through the nozzle generates thrust. Hypersonic airbreathing vehicles also hold the promise of low-cost access to space and a possible choice for the next generation of high-speed transportation. Because of the significant promise, it is not surprising that hypersonic research has achieved significant milestones recently, including the sustained flight at around Mach 6–7 for 210 s of the X-51A vehicle [2,3]. To achieve conditions that enable autoignition, the air captured by the engine has to achieve high temperatures and pressures: a task that is partially accomplished through a sequence of carefully designed shock waves anchored to the vehicle forebody and within the isolator chamber.

The scramjet is a mechanically simple and potentially robust alternative to conventional engines, as there are no moving parts; although its minimum flight speed is fixed by the requirement of reaching supersonic flow at the entrance of the combustor (downstream of the forebody compression). On the other hand, maximum thrust generation is a direct consequence of optimal mixing and heat

release in the combustor and is directly proportional to the fuel flow rate. The design of a scramjet system is complicated by the existence of thermodynamic, structural, combustion, and fluid-dynamic limits to the amount of fuel that can be burnt in the combustor. The thermodynamic limit is associated with the inability to sustain supersonic flow in a duct with arbitrary heat addition. Above a certain threshold (which is typically referred to as the thermal choking limit), a normal shock wave is formed in the combustor and the downstream flow becomes subsonic. The combustion limit is associated with the stoichiometry of the fuel/air mixture, while the fluid-dynamic limit is imposed by the blockage induced by the added fuel mass in the chamber and the possibility of creating large areas of flow separation near the injectors. Finally, the structural limit is related to the properties (strength and heat capacity/conductivity of the material) used to build the combustor section. It is worth noting that these limits are related to critical and possibly irrecoverable failures of the system.

The performance of a scramjet engine is carefully tuned to achieve the highest level of thrust that is compatible with a specified safety margin (which is defined as the distance between the design condition and a critical failure). Computational tools are routinely used in aerodynamic design and to predict the heat release resulting from combustion [4,5]. These simulations are capable of achieving high levels of accuracy by incorporating detailed representations of the underlying physical processes. This typically leads to a large increase in computational costs that can limit the number of configurations that can be analyzed. On the other hand, the characterization of the risks relies on the identification of the uncertainties present in the real operating vehicle and the determination of the corresponding induced variability of the flow conditions within the scramjet. A formal reliability analysis requires the determination of the probability of failure of the system that, in turn, involves the analysis of a large number of possible operating scenarios. With this many samples required by a brute-force risk analysis method, using high-fidelity physics-based computational tools may be infeasible.

In the present work, we present an approach that can enable accurate risk analysis of hypersonic flows using a physics-based computational tool. We demonstrate this methodology in estimating the probability of unstart of a scramjet engine under uncertain conditions using a computational model described in Sec. II. Unstart is a phenomenon that can be caused by multiple factors (including thermal choking) in which the well-established shock train in the inlet-isolator moves abruptly upstream, dramatically reducing the mass flow rate through the scramjet engine and virtually rendering the engine unusable. A Monte Carlo approach is pursued, but the computational cost of the analysis is greatly reduced by applying

adjoint-based stratified sampling techniques. Significant reductions in the computational cost of the simulations (up to a factor of 5) are achieved using this new methodology.

II. Simulation Model

All computations are performed using the unstructured mesh compressible flow solver Joe [6]. While Joe is capable of solving the unsteady Reynolds-averaged Navier–Stokes equations (RANS) with various turbulence models, in this work, we use its Euler capabilities with a second-order-accurate cell-centered discretization for the inviscid fluxes. An idealized two-dimensional version of the HyShot II scramjet geometry that has been both flight and ground tested [7,8] will be studied. The isolator, combustor, and nozzle of the test vehicle (Fig. 1) is replicated by the geometry used in our simulation (Figs. 2 and 3).

The inflow to the isolator is approximately at Mach $M_2 = 2.7$ and corresponds to the flow after it has been deflected by two shocks from the forebody and cowl in the real vehicle, calculated by solving the oblique shock equations [9]. The first oblique shock equation is solved with turning angles $\theta_N + \alpha$, where $\theta_N = 18^\circ$ is the angle of the nose wedge and α is the angle of attack, for the shock angle β_1 and flow properties M_1 , p_1 , and ρ_1 after the nose shock. The second oblique shock equation is solved with turning angle θ_N for the shock angle β_2 and flow properties M_1 , p_1 , and ρ_1 after the cowl shock. The flow after this second shock represents the inflow condition of the combustor channel.

Since the flow entering the simulation domain is the flow downstream of the cowl, the inlet velocity will always be parallel to the combustor walls. Any changes to the vehicle angle of attack α will thus translate to changes in the inlet flow variables. A shock train is generated by a blunt lip at the entrance of the lower wall of the isolator, as seen in Fig. 2. The simulations are run in an inviscid mode, and a simple heat-release model [10] is used to mimic the combustion process. In this model, the cumulative heat release is simply added as a one-dimensional source term to the energy equation. The heat release (in joules per second) is given by

$$Q = \phi f_{st} H_f m_{air} \eta(x/L_c) \quad (1)$$

where $\eta(x/L_c) = 1 - e^{-(C_c x/L_c)^{D_c}}$ is the heat-release distribution function. The various parameters used in the above expressions are summarized in Table 1. The shape parameter D_c is tuned to achieve a good fit with the ground-based experimental measurements of the DLR [8]. The addition of the heat release was seen to accelerate the flow and increase the number of shocks in the combustor (these were

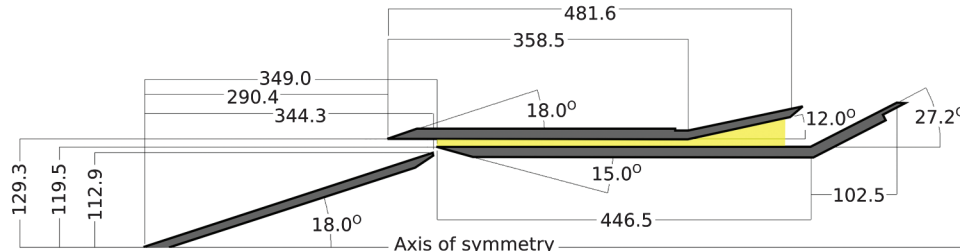


Fig. 1 Geometry of the Hyshot vehicle. The yellow region represents the area of the flow simulation.

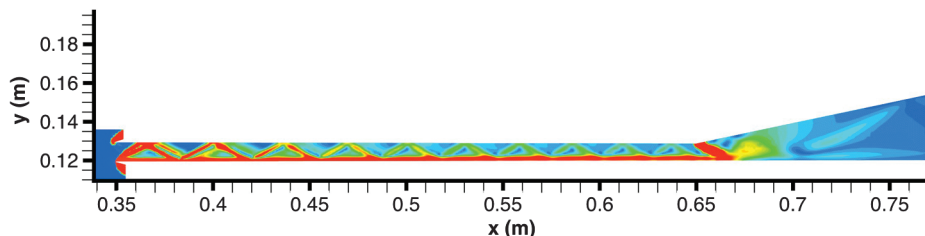


Fig. 2 Simulation domain for HyShot II scramjet. Contours of density gradient magnitude are shown for a case with fuel injection.

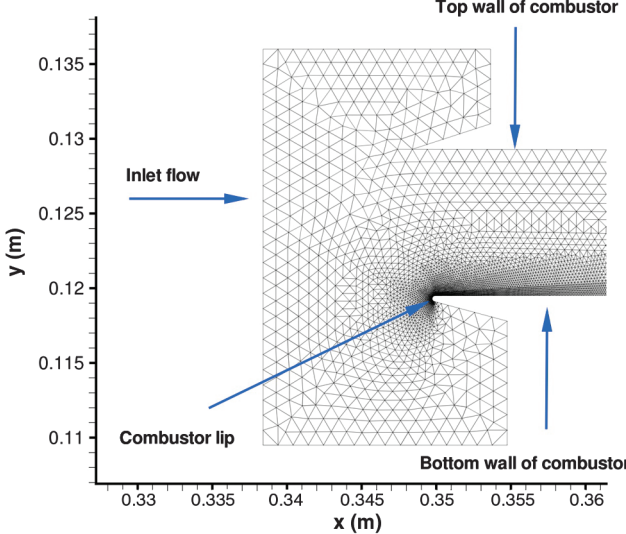


Fig. 3 Mesh near the inlet.

Table 1 Summary of parameters used in heat-release model

Symbol	Definition	Baseline value
ϕ	Equivalence ratio	0.3
f_{st}	Stoichiometric fuel/air ratio	0.028
H_f	Fuel heating value (H_2)	120 MJ/kg
L_c	Combustor length	0.368 m
K_c	Fraction of completed combustion	0.95
D_c	Shape parameter	0.75
C_c	Shape parameter	$-\log(1 - K_c)^{1/D_c}$
X_c	Combustion ignition position	0.418 m

also found to be increasing in frequency toward the exit of the combustor). A nominal comparison with experimental data is shown in Fig. 4, where the validity of the inviscid model is demonstrated. The mesh used in the study consisted of 80,000 control volumes, and the typical time to perform one simulation was about 8 min. on one processor. In a practical hypersonic aircraft, the use of the term unstart may refer to either of the following scenarios: 1) inefficient mass capture of the inlet due to offdesign operation, or 2) combustion-driven disgorging of the shock train structure from the isolator into the inlet. In this work, simulations target the latter

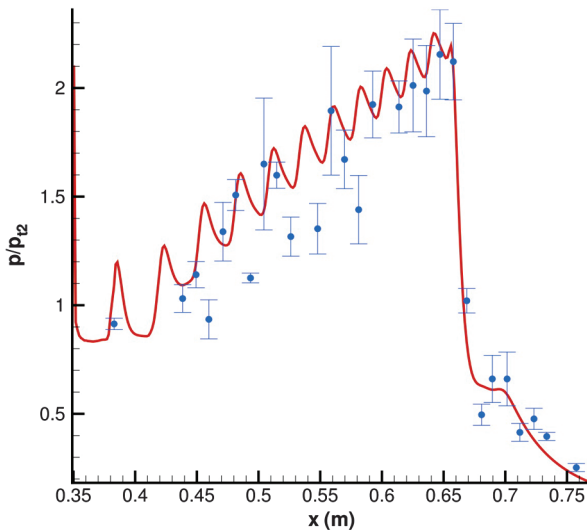


Fig. 4 Normalized pressure on lower wall of simulated HyShot II isolator/combustor (lines: present computations; dots with error bars: DLR measurements [8]). Error bars are mostly due to unsteadiness during measurements.

type of unstart, which is a result of the heat release Q crossing a certain threshold, resulting in a large region of subsonic flow and subsequent upstream propagation of the shock system.

III. Discrete Adjoint Formulation for Gradient Computation

The adjoint procedure [11] is an efficient method to compute the variation of a functional \mathcal{J} with respect to a large number of parameters. In the discrete adjoint approach [12,13], the adjoint equations are directly derived from the discretized form of the governing equations. Let $R(U, w) = 0$ represent the governing equations in a domain Ω that is to be solved for flow variables U in the presence of one or more uncertain parameters w . Typically, we will be interested in the values of a functional $\mathcal{J}(U, w)$, its variations with respect to the parameters w , and its moments. As will be explained later in this paper, the value of the gradient vector of this functional can be used in the risk assessment procedure described in this work. When solved numerically on a mesh Ω_H , a discretized form of the governing equations $R_H(U_H, w) = 0$ is used to compute a discrete functional $\mathcal{J}(U_H, w)$ [14,15]. The variation of this discrete functional with respect to some change in the uncertain parameters δw is given by

$$\delta \mathcal{J} = \left(\frac{\partial \mathcal{J}}{\partial w} + \frac{\partial \mathcal{J}}{\partial U_H} \frac{\partial U_H}{\partial w} \right) \delta w \quad (2)$$

This variation can be evaluated if $\frac{\partial U_H}{\partial w}$ is known, and this can be determined, for instance, by linearizing the governing equations, $R_H(U_H, w) = 0$, and solving the resulting expression for $\frac{\partial U_H}{\partial w}$:

$$\frac{\partial R_H}{\partial w} + \frac{\partial R_H}{\partial U_H} \frac{\partial U_H}{\partial w} = 0 \quad (3)$$

The above equation must be solved iteratively, and the computational effort is comparable to solving the governing equation $R_H = 0$. Since Eq. (3) has to be solved for every component w_i , this direct approach will be expensive if a large number of parameters are present in w . To circumvent this computational expense, the adjoint approach is useful; by introducing the adjoint variable Ψ as a Lagrange multiplier, we can write

$$\begin{aligned} \delta \mathcal{J} &= \left(\frac{\partial \mathcal{J}}{\partial w} + \frac{\partial \mathcal{J}}{\partial U_H} \frac{\partial U_H}{\partial w} + \Psi_H^T \left[\frac{\partial R_H}{\partial w} + \frac{\partial R_H}{\partial U_H} \frac{\partial U_H}{\partial w} \right] \right) \delta w \\ &= \left(\frac{\partial \mathcal{J}}{\partial w} + \Psi_H^T \frac{\partial R_H}{\partial w} \right) \delta w \end{aligned} \quad (4)$$

provided

$$\left[\frac{\partial R_H}{\partial U_H} \right]^T \Psi_H = - \left[\frac{\partial \mathcal{J}}{\partial U_H} \right]^T \quad (5)$$

Equation (5) is called the discrete adjoint equation because its derivation proceeds directly from the discretized form of the governing equations. Note that, unlike Eq. (3), Eq. (5) does not contain derivatives with respect to w . It only contains derivatives of the discrete functional \mathcal{J} . This means that, irrespective of the dimension of w , we have to solve just one adjoint equation for each discrete functional of interest; the full gradient is then obtained from Eq. (4), which only requires dot products and hence is computationally inexpensive. With this approach, the expense of computing the full gradient is roughly comparable to that of one additional flow solution. In this work, the software suite ADOL-C [16] has been used for automatic differentiation [17]. In this approach, the user specifies independent and dependent variables and marks a section of the code to be differentiated. Operator overloading is employed to perform the differentiation process in reverse mode.

IV. Risk Quantification

Risk analysis for both the initial phase of the flight [18] and the overall trajectory [19], as well as some aspects of the unstart control hardware [20], have previously been carried out for the X-43A hypersonic vehicle. These studies are based on simplified computational models that rely heavily on empirical correlations to predict system behavior. Uncertainties in the operating scenarios (atmospheric state, vehicle flight conditions, controls, etc. (namely, aleatoric uncertainties [21]) were typically characterized using Gaussian probability distributions and propagated through the computational model using brute-force Monte Carlo sampling. In spite of the demonstrated success of this approach, there is a need to reduce the cost and effort involved in calibrating the computational models to allow a more comprehensive exploration of the design space and to extend the performance threshold closer to the operability limits by reducing excessively the conservative use of the safety factors while demonstrating reliability in expected variations in the operation of the vehicles.

In this work, we offer an alternative approach to reliability analysis in which the computational model includes a refined representation of the shock dynamics within the engine but with a lower-fidelity approximation to the mixing and combustion processes combined in a simplified heat-release model. Following the approach introduced by Iaccarino et al. [22], instead of using empirical data to correlate the heat-release predictions, we introduce additional uncertain quantities such as the ignition location, amount of fuel burnt, etc., that do not represent the variability encountered during the operation of the actual vehicle (aleatory uncertainties) but rather indicate a lack of knowledge regarding the detailed physical processes (these are termed epistemic uncertainties [21]). In addition, the number of overall simulations required to investigate the probability of failure is reduced by using sensitivity information obtained through the use of adjoint methods. Sensitivity derivatives have been used before in hypersonic problems to help design scramjet inlets [4] leading to optimal geometrical shapes for the cowl and one-dimensional thermodynamic equations. The connection between sensitivity derivatives and the approximate representation of the probability of failure has been exploited in reliability estimation methods (see for example [23]); here, we use the sensitivity information in an alternative way. Recently, Wang [24] used the adjoint method to compute sensitivity derivatives and to formulate an acceleration strategy to concentrate Monte Carlo samples toward the tail of the output probability distributions. In this paper, we apply this technique to the evaluation of the probability of unstart due to thermal choking.

V. Formulation of the Risk Assessment Problem

The problem is to compute the probability that unstart initiates in the scramjet engine, given probability distributions in the following five uncertain parameters: 1) angle of attack of the vehicle, 2) ambient temperature at a pressure altitude of 27,000 m, 3) combustion shape parameter that describes the shape of the supersonic heat release in the combustor [D_c in Eq. (1)], 4) combustor burning fraction describing the percentage of fuel that is burnt in the combustor (K_c in Table 1), and 5) combustor ignition position describing the position where the fuel first ignites, after the fuel injection at 0.408 m.

We denote this set of input uncertain parameters by the vector w .

A. Quantitative Definition of Unstart

Unstart in scramjet engines is characterized by the formation of a strong normal shock wave in the combustor. This shock wave propagates upstream toward the inlet and eventually reduces significantly the mass flow rate and the thrust generated by the engine. The existence of the strong shock wave can be identified by sensing the difference between the maximum pressure in the combustor and the inlet pressure. In practice, we find that a high-order norm of the combustor wall pressure serves as a very good approximation to the maximum pressure in identifying the existence of the unstart normal shock wave. This metric is preferred because a polynomial norm is a smoother functional than the maximum norm, which can be discontinuous in the context of many shock waves of almost equal strength, and this in turn makes the functional gradient better behaved.

In this problem, we use the eighth norm of the combustor upper-wall pressure (at a prespecified simulation time) as the quantitative identifier of unstart. This functional is given by

$$\mathcal{J} = \left(\int_{W_U} (p - p_I)^8 ds \right)^{1/8} \quad (6)$$

where W_U denotes the upper wall of the combustor. This wall pressure is relative to the combustor inlet pressure p_I and is normalized with respect to the inlet density ρ_I and the square of the velocity U_I of a reference configuration. The reference configuration is defined as the one that is achieved when all the uncertain input parameters take the value of the mean of their respective distributions. Note that \mathcal{J} is a function of w through the dependence of p on w expressed by the governing equations of the flow.

These quantities are computed at the simulation time when a fluid particle at the combustor inlet velocity has traveled 2.4 m, approximately eight times the length of the combustion chamber. For all conditions that we observed to finally cause unstart, a normal shock wave had formed at this simulation time, causing an abnormally high pressure peak inside the combustion chamber. As mentioned earlier, the objective function \mathcal{J} represents the eighth norm of the combustor wall pressure. It is a weighted averaged of the combustor wall pressure, with higher weight toward the higher pressure regions; therefore, it serves as a good indicator of this abnormally high pressure peak, the precursor of unstart.

With this objective function $\mathcal{J}(w)$ serving as an indicator, we find that the critical value of the objective function beyond which we expect unstart, or

$$\mathcal{J}_{\text{critical}} = \mathcal{C} = 0.23 \quad (7)$$

separates the operating scramjet cases and the unstart cases very clearly. We observe that conditions exceeding this critical value indicate the presence of a normal shock in the combustor, eventually causing unstart; conditions below this critical value reach a steady state for a normal operating condition. Based on this observation, we define $\{w | \mathcal{J}(w) > \mathcal{C}\}$ as the region of the uncertain input parameter space that causes unstart and $\{w | \mathcal{J}(w) < \mathcal{C}\}$ as the region of the uncertain input parameter space that ensures normal (or started) scramjet operation. Based on this criteria, the formal statement of the problem formulation is to calculate the unstart probability

$$\mathbb{P}(\{w | \mathcal{J}(w) > \mathcal{C}\}) \quad (8)$$

Table 2 Summary of input uncertain parameters

Parameter	Mean	Standard dev	Probability distribution
Vehicle angle of attack α	0°	2°	Normal distribution
Ambient temperature T_A	223.5 K	10.0 K	Lognormal, minimum 0 K
Combustion shape parameter D_c	0.75	0.05	Beta, [0, 1]
Combustion burning fraction K_c	0.95	0.03	Beta, [0, 1]
Combustion ignition position X_c	0.418 m	0.010 m	Lognormal, minimum 0.408 m
Ambient pressure p_A	Deterministic at pressure altitude of 27,000 m: 2.188 kPa		
Freestream Mach number	Deterministic at Mach 7.5		

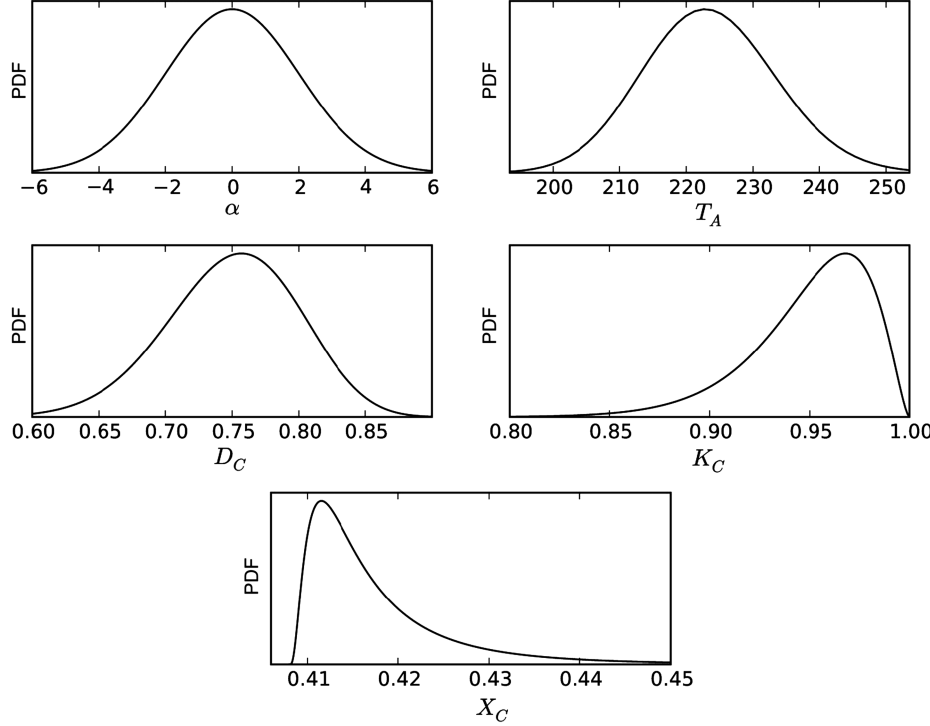


Fig. 5 Probability density function of input uncertain parameters.

where the objective function \mathcal{J} and the critical value \mathcal{C} are defined as explained previously.

B. Probability Distribution of Uncertain Input Parameters

In this work, the chosen distributions of these uncertain parameters are summarized in Table 2 but the methodology described in this paper is able to handle arbitrary probability density functions that may be obtained from additional knowledge of the priors. Figure 5 shows the probability density functions chosen for these parameters. We choose a lognormal distribution for the ambient temperature T_A because the temperature (in degrees Kelvin) must be positive. Similarly, the position of ignition X_C must occur after the fuel injection, which is located at 0.408 m measured from the nose of the entire vehicle. Therefore, we prescribe a lognormal random variable with minimum 0.408 m. The combustor shape parameter D_C and burning fraction K_C are numbers between 0 and 1. Therefore, we use Beta distributions to describe these random variables.

The distributions of these uncertain parameters are chosen so that their standard deviation matches what we consider reasonable for the

Hyshot vehicle. However, because we do not have detailed knowledge of their probability distributions, the specified shape of the distributions can be inaccurate. We also assume that these input parameters are independent of each other. This assumption should be modified if more information on the uncertain parameters are available (e.g., via statistical inference of available data). Our method for computing the unstart probability presented in this paper is based on sampling of both the computational model and the linear surrogate. Therefore, it can be generalized to correlated input random variables with other distributions, as long as samples of the input random variables can be computationally generated.

Since the inflow to the computation domain corresponds to the flow after the forebody and cowl shocks, the uncertainties in the angle of attack and ambient temperature translate into uncertainties in pressure, density, temperature and velocity at the inflow of the computational domain. The input uncertainties in these parameters are calculated by using the oblique shock jump conditions and are nondimensionalized with a reference velocity of 1882 m/s, a reference density 0.368 kg/m³, and a reference pressure 1223 kPa.

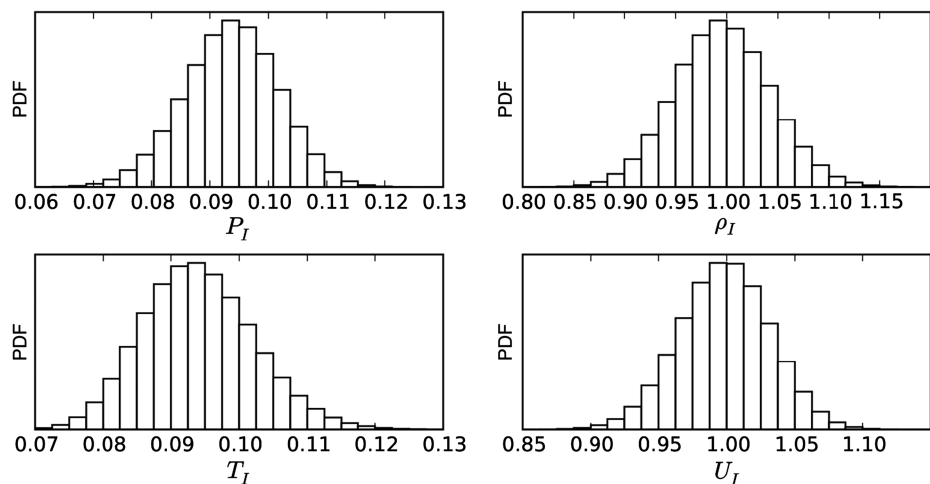


Fig. 6 Empirical probability density function of uncertain parameters in the inflow condition, calculated from samples of α and T_A by solving the oblique shock equations twice.

The probability density functions of these inlet uncertain parameters, as input to the computational fluid dynamics calculation, are shown in Fig. 6.

VI. Naive Monte Carlo Method

The problem posed in Sec. V, computing the probability that unstart initiates in the scramjet engine, can be solved using the naive Monte Carlo method. The naive Monte Carlo method takes N samples of the uncertain input parameters w_1, \dots, w_N and performs a flow solution for each sample. The samples of uncertain input parameters are drawn according to distributions described in Sec. V.B. The objective function $\mathcal{J}(w_k)$ is then computed for each $k = 1, \dots, N$. The probability of unstart is then estimated as the fraction of unstarted cases in the sampled simulations

$$\mathbb{P}(\mathcal{J}(w) > \mathcal{C}) \approx P_N^{mc} = \frac{1}{N} \sum_{k=1}^N I_{\mathcal{J}(w_k) > \mathcal{C}} \quad (9)$$

where

$$I_{\mathcal{J}(w) > \mathcal{C}} = \begin{cases} 1, & \mathcal{J}(w) > \mathcal{C} \\ 0, & \mathcal{J}(w) < \mathcal{C} \end{cases} \quad (10)$$

Figure 7 shows a histogram of the objective function $\mathcal{J}(w_i)$ with 3000 samples computed from numerically solving the Euler equation 3000 times. We can see from the plot that the critical value separates two distinct groups: the majority of the samples lie to the left of the critical value and are normal operating scramjets, and a small portion

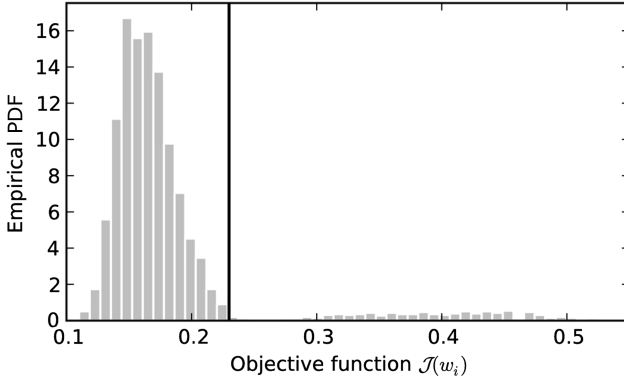


Fig. 7 Empirical probability density function (PDF) of the objective function \mathcal{J} based on 3000 naive Monte Carlo samples. The vertical line indicates the critical value $\mathcal{C} = 0.23$. Samples on the left of this line are normal operating cases, and samples on the right of this line are unstarted cases.

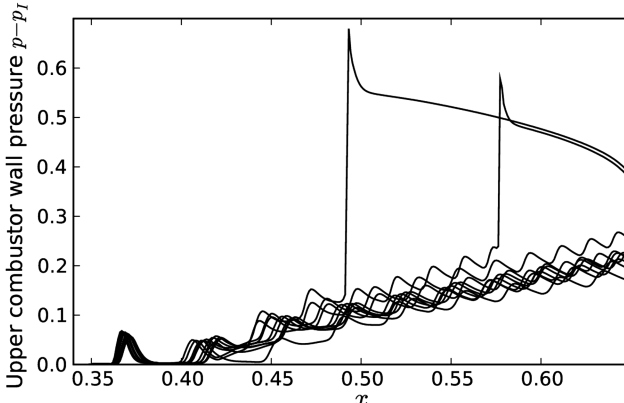


Fig. 8 Combustor upper-wall pressure corresponding to the first 10 Monte Carlo samples in Fig. 7. Eight out of the 10 samples are normal operating scramjets; the two samples with sharp peaks, indicating normal shock waves in the combustor, are developing unstart.

Table 3 Summary statistics of naive Monte Carlo sampling

Number of samples	Estimated unstart probability	Estimator variance	2σ confidence interval
1000	0.073	6.8×10^{-5}	(0.057, 0.089)
2100	0.083	3.6×10^{-5}	(0.071, 0.095)
3000	0.082	2.5×10^{-5}	(0.072, 0.092)

of samples are seen to the right of the critical value. The high value of the objective function of these samples indicates the existence of strong normal shock waves in the corresponding flowfields, as shown in Fig. 8. The probability of unstart calculated using this naive Monte Carlo method for three different numbers of samples N is shown in Table 3. Since P_N^{mc} in Eq. (9) is an unbiased estimator, the mean square error of the estimator is equal to its variance. The variance of P_N^{mc} can be estimated by

$$\text{Var}(P_N^{mc}) = \text{Var}\left(\frac{1}{N} \sum_{k=1}^N I_{\mathcal{J}(w_k) > \mathcal{C}}\right) = \frac{\text{Var}(I_{\mathcal{J}(w_k) > \mathcal{C}})}{N} \quad (11)$$

Because $I_{\mathcal{J}(w_k) > \mathcal{C}}$ is a Bernoulli random variable, for which the parameter is estimated with

$$\mathbb{P}(I_{\mathcal{J}(w_k) > \mathcal{C}} = 1) = \mathbb{P}(\mathcal{J}(w_k) > \mathcal{C}) \approx P_N^{mc} \quad (12)$$

its variance can be estimated with

$$\begin{aligned} \text{Var}(I_{\mathcal{J}(w_k) > \mathcal{C}}) &= \mathbb{P}(I_{\mathcal{J}(w_k) > \mathcal{C}} = 1) - \mathbb{P}(I_{\mathcal{J}(w_k) > \mathcal{C}} = 0)^2 \\ &\approx P_N^{mc} - P_N^{mc}^2 \end{aligned} \quad (13)$$

Therefore, the variance of the estimator P_N^{mc} can be estimated as

$$\text{Var}(P_N^{mc}) \approx \frac{P_N^{mc} - P_N^{mc}^2}{N} \quad (14)$$

This variance estimates, together with the resulting 2σ confidence interval of the unstart probability, are given in Table 3 for $N = 1000$, 2100, and 3000.

VII. Adjoint Approximation

Both the flow and the adjoint equations are solved at a reference condition w_0 , where all the uncertain input parameters take on their respective mean values (Table 2):

$$\begin{aligned} w_0 &= F(\alpha_0, T_{A0}, D_{C0}, K_{C0}, X_{C0}) \\ &= F(0^\circ, 223.5 \text{ K}, 0.75, 0.95, 0.418 \text{ m}) \end{aligned} \quad (15)$$

where F represents the solution of two oblique shock equations, which map the uncertain input parameters to the uncertain combustor inlet conditions. From the flow solution, we compute the objective function $\mathcal{J}(w_0)$. Using the adjoint solution, we can compute the derivative of the objective function \mathcal{J} with respect to each uncertain input random variable. In other words, we compute the adjoint sensitivity gradient $\nabla \mathcal{J}(w_0)$. The computed sensitivity gradient is given in Table 4. With this adjoint sensitivity gradient, we construct a linear approximation to the objective function

Table 4 Adjoint sensitivity gradient with respect to the uncertain input parameters

Variable	Gradient
K_C	0.383
D_C	0.160
X_C	-0.593
ρ_I	-0.106
p_I	0.722
T_I	0.000
U_I	-0.413

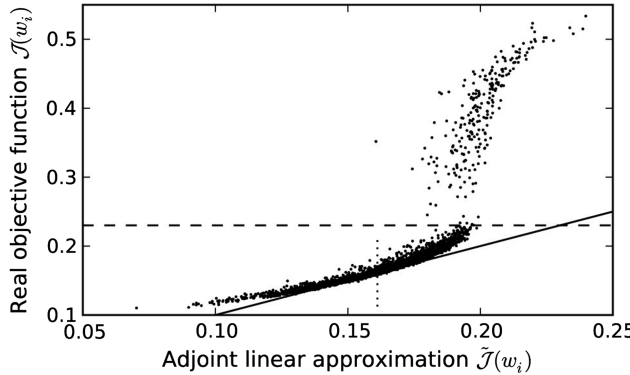


Fig. 9 Adjoint approximation for the 3000 naive Monte Carlo samples, plotted against the real/computed value of the objective function. The solid line indicates the exact approximation of $\mathcal{J} = \tilde{\mathcal{J}}$. The objective function of the reference configuration $\mathcal{J}(w_0) = \tilde{\mathcal{J}}(w_0)$ is indicated by the vertical dotted line.

$$\mathcal{J}(w) \approx \tilde{\mathcal{J}}(w) = \nabla \mathcal{J}(w_0) \cdot (w - w_0) + \mathcal{J}(w_0) \quad (16)$$

This adjoint linear approximation $\tilde{\mathcal{J}}(w_i)$, where the samples w_1, \dots, w_{3000} are used in the last section, are plotted in Fig. 9 against the real objective function $\mathcal{J}(w_i)$. The linear approximation (based on one gradient evaluation) has an average of 20% error when the engine is in normal operation and up to 15% error when the engine unstarts. The large error indicates a strong nonlinearity in the problem, which is directly a consequence of the existence of strong nonlinearities in the flow and the bifurcation nature of the unstart phenomenon.

Despite its limitations, the linear approximation correlates well with the real objective function and is useful in identifying the trend. A configuration w is much less likely to unstart when the value of the linear approximation of $\tilde{\mathcal{J}}(w)$ is small. At a configuration w where the value of the linear approximation $\tilde{\mathcal{J}}(w)$ is large, the engine almost always experiences unstart. This observation is the key motivation for using the adjoint-computed gradients to accelerate the Monte Carlo method for estimating the unstart probability $\mathbb{P}(\mathcal{J} > C)$, taking advantage of both the small computational cost of evaluating the adjoint approximation (16) and the strong correlation between $\tilde{\mathcal{J}}$ and \mathcal{J} .

VIII. Adjoint-Based Stratified Sampling

A. Adjoint-Based Stratification

We separate the samples into three strata based on the value of the adjoint linear approximation $\tilde{\mathcal{J}}$:

1) *Safe stratum*: In this group, the adjoint approximation predicts with high probability that the scramjet engine does not unstart.

2) *Uncertain stratum*: In this group, the adjoint approximation is unable to predict with confidence whether the scramjet engine unstarts or not.

3) *Unstart stratum*: In this group, the adjoint approximation predicts with high probability that the scramjet engine unstarts.

The boundaries of these three groups are determined by taking 100 preliminary samples of the uncertain parameters w_1, \dots, w_{100} and performing a flow solution on each of the 100 samples. From the flow solutions, the objective function $y_i = \mathcal{J}(w_i)$, $i = 1, \dots, 100$, is calculated. Based on whether this objective function exceeds the set threshold C , the 100 preliminary samples are categorized into safe and unstart samples.

The adjoint approximation of the objective function, $x_i = \tilde{\mathcal{J}}(w_i)$, $i = 1, \dots, 100$, is also computed for these 100 samples. For both the safe and unstart samples, we compute the mean and standard deviation. In other words, we compute the sample mean μ_{x1} and standard deviation σ_{x1} of $\{x_i | y_i < C\}$, and the sample mean μ_{x2} and standard deviation σ_{x2} of $\{x_i | y_i > C\}$.

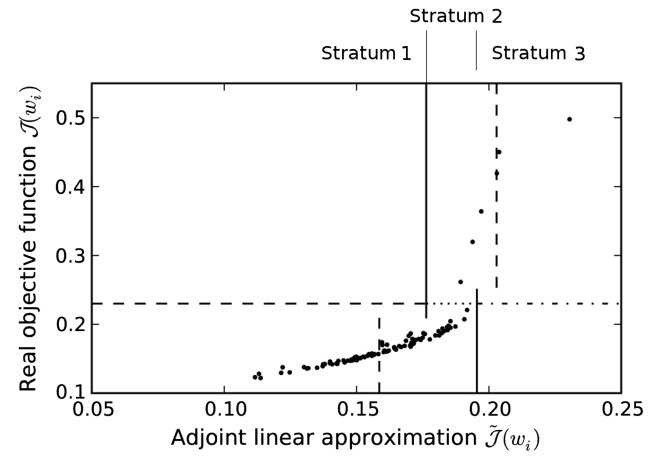


Fig. 10 Stratification scheme using flow solutions and adjoint approximations of 100 samples.

Based on the mean and standard deviation of these two groups, we define the boundary between the three strata for the stratified sampling algorithm. The safe stratum is defined as

$$S_1 = \{w | \tilde{\mathcal{J}}(w) < \mu_{x2} - 2\sigma_{x2}\} \quad (17)$$

the unstart stratum is defined as

$$S_3 = \{w | \tilde{\mathcal{J}}(w) > \mu_{x1} + 2\sigma_{x1}\} \quad (18)$$

and the uncertain stratum is defined as

$$S_2 = \{w | \mu_{x2} - 2\sigma_{x2} < \tilde{\mathcal{J}}(w) < \mu_{x1} + 2\sigma_{x1}\} \quad (19)$$

The stratification scheme is illustrated in Fig. 10. In this figure, dots represent the 100 Monte Carlo samples used to construct the stratification. The horizontal line indicates the boundary between operating safe and unstart cases. The lower left vertical dashed line indicates the sample mean of the adjoint approximation $\tilde{\mathcal{J}}$ of the operating cases, and the upper right vertical dashed line indicates the sample mean of the adjoint approximation $\tilde{\mathcal{J}}$ of the unstart cases. The lower solid vertical line indicates the right two-standard-deviation boundary of the operating cases, and the upper solid vertical line indicates the left two-standard-deviation boundary of the unstart cases. These two solid lines separate the sample space into three strata based on the adjoint approximation: the dashed part of the horizontal line indicates stratum 1, the safe stratum; the dotted part of the horizontal line indicates stratum 2, the uncertain stratum; and the dashed-dotted part of the horizontal line indicates stratum 3, the unstart stratum. The boundaries between these strata are 0.176 and 0.195, respectively. Details of the resulting stratification are given in row 3 of Table 5.

B. Calculation of the Unstart Probability

The following three steps are used to calculate the unstart probability using our adjoint-based stratified sampling:

1) Calculate the probability that a sample falls into each stratum,

$$\mathbb{P}(w \in S_i), \quad i = 1, 2, 3 \quad (20)$$

These probabilities are calculated by computing the adjoint approximation for $N_A = 13,160,000$ samples w and determining the fraction of samples that lie in each stratum S_i :

$$\mathbb{P}(w \in S_i) \approx P_i^{(1)} = \frac{1}{N_A} \sum_{k=1}^{N_A} I_{w_k \in S_i}, \quad i = 1, 2, 3 \quad (21)$$

where

Table 5 Summary statistics of adjoint-based stratified sampling computation

	Stratus		
	Started	Uncertain	Unstart
i	1	2	3
$\{\tilde{\mathcal{J}}(w) w \in S_i\}$	$(-\infty, 0.17635)$	$(0.17635, 0.19548)$	$(0.19548, +\infty)$
$P_i^{(1)} \approx \mathbb{P}(w \in S_i)$	0.74741	0.19521	0.05738
Variance of $P_i^{(1)}$	$<1.9 \times 10^{-8}$	$<1.9 \times 10^{-8}$	$<1.9 \times 10^{-8}$
Number of flow solutions N_i	1495	390	115
Number of unstart flow solutions	2	48	114
$P_i^{(2)} \approx \mathbb{P}(\mathcal{J}(w) > \mathcal{C} w \in S_i)$	0.0014	0.123	0.9913
Estimator variance of $P_i^{(2)}$	8.9×10^{-7}	0.000277	0.000075
Contribution to the variance of P^{ss}	5.0×10^{-7}	1.05×10^{-5}	2.5×10^{-7}
$P^{ss} \approx \mathbb{P}(\mathcal{J}(w) > \mathcal{C})$		0.082	
Estimator variance of P^{ss}		1.13×10^{-5}	
2σ confidence interval of P^{ss}		(0.075, 0.089)	
Total number of flow solutions			2100

$$I_{w_k \in S_i} = \begin{cases} 1, & w_k \in S_i \\ 0, & w_k \notin S_i \end{cases} \quad (22)$$

Because each stratum is defined in terms of the adjoint approximation $\tilde{\mathcal{J}}$, calculating the probabilities involves only sampling the uncertain parameters w , and calculating the adjoint linear approximation $\tilde{\mathcal{J}}$. Since the computational cost of sampling $\tilde{\mathcal{J}}$ is negligible compared with sampling \mathcal{J} , we can use as many samples as necessary to keep the error in the calculated $\mathbb{P}(w \in S_i)$ under a desired level.

In our calculations, we used 13,160,000 samples to calculate these probabilities. As shown in Sec. VIII.C, the resulting statistical variances in these probability estimates are orders of magnitude lower than the variance in the conditional probability calculated in step 2. Therefore, the errors in the computed probabilities are negligible in our analysis (see Fig. 11). The calculated probabilities and variance estimates are given in rows 4 and 5 of Table 5.

2) Calculate the conditional probability of unstart, given that a sample falls into each stratum

$$\mathbb{P}(\mathcal{J}(w) > \mathcal{C} | w \in S_i), \quad i = 1, 2, 3 \quad (23)$$

We perform flow solutions on 2000 samples. The number of samples in the three strata N_1 , N_2 , and N_3 is chosen to be proportional to the probability of the stratum, calculated in step 1. The samples w_k^i , $k = 1, \dots, N_i$, $i = 1, 2, 3$, are generated by obtaining a large number of samples and selecting the first N_i samples that lie in stratum i .

The conditional probability of unstart occurring in each stratum is estimated as the fraction of unstarted cases in that stratum. In other words, we estimate

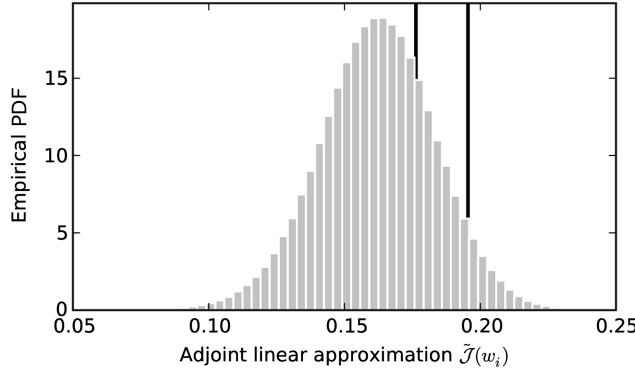


Fig. 11 Calculating the probability of each stratum by calculating the adjoint linear approximation of 13,160,000 samples. The gray histogram shows the empirical PDF derived from the large number of samples. The two vertical lines show the boundary between the three strata.

$$\mathbb{P}(\mathcal{J}(w) > \mathcal{C} | w \in S_i) \approx P_i^{(2)} = \frac{1}{N_i} \sum_{k=1}^{N_i} I_{\mathcal{J}(w_k^i) > \mathcal{C}} \quad (24)$$

where

$$I_{\mathcal{J}(w_k) > \mathcal{C}} = \begin{cases} 1, & \mathcal{J}(w_k) > \mathcal{C} \\ 0, & \mathcal{J}(w_k) \leq \mathcal{C} \end{cases} \quad (25)$$

The number of samples in each stratum N_i , the number of unstarted solutions, and the calculated conditional probabilities are shown in rows 6, 7, and 8 of Table 5.

3) Calculate the probability of unstart

$$\begin{aligned} \mathbb{P}(\mathcal{J}(w) > \mathcal{C}) &= \sum_{i=1}^3 \mathbb{P}(w \in S_i) \mathbb{P}(\mathcal{J}(w) > \mathcal{C} | w \in S_i) \\ &\approx P^{ss} = \sum_{i=1}^3 P_i^{(1)} P_i^{(2)} \end{aligned} \quad (26)$$

This probability estimate is shown in row 11 of Table 5.

C. Confidence Interval of Unstart Probability Estimates

We first analyze the error in estimator $P_i^{(1)}$ in Eq. (21). Because $\mathbb{P}(w \in S_i) = \mathbb{E}(I_{w_k \in S_i})$, where \mathbb{E} indicates the expectation, the estimator is unbiased, and the error is solely from the variance (see Fig. 12):

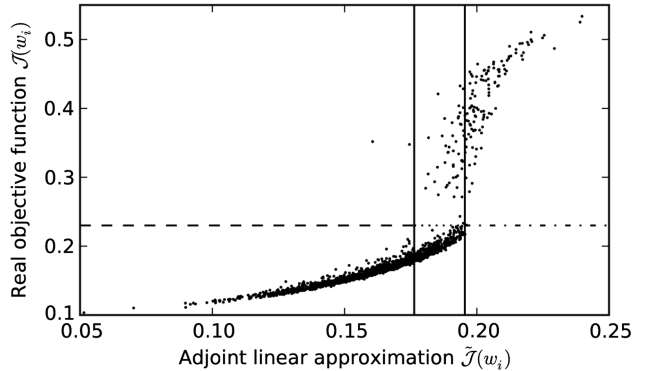


Fig. 12 Stratified sampling with actual flow solutions on 2000 samples. The horizontal line indicates the boundary between operating/start cases and unstart cases. The vertical lines indicate the boundaries between the three strata: the dashed part of the horizontal line indicates stratum 1, the started stratum; the dotted part of the horizontal line indicates stratum 2, the uncertain stratum; and the dashed-dotted part of the horizontal line indicates stratum 3, the unstart stratum.

$$\begin{aligned} \text{Var}(P_i^{(1)}) &= \text{Var}\left(\frac{1}{N_A} \sum_{k=1}^{N_A} I_{w_k \in S_i}\right) = \frac{\text{Var}(I_{w \in S_i})}{N_A} \\ &= \frac{\mathbb{P}(w \in S_i) - \mathbb{P}(w \in S_i)^{(2)}}{N_A} < 1.9 \times 10^{-8} \end{aligned} \quad (27)$$

for $N_A = 13,160,000$. This is negligible compared with the variance of estimating the conditional probabilities, as shown in Table 5.

We next estimate the error in the estimator $P_i^{(2)}$ of the conditional probabilities in Eq. (24). It is also an unbiased estimator, and its mean square error, which is equal to the variance, is

$$\begin{aligned} \text{Var}(P_i^{(2)}) &= \text{Var}\left(\frac{1}{N_i} \sum_{k=1}^{N_i} I_{\mathcal{J}(w_k^i) > C}\right) = \frac{\text{Var}(I_{\mathcal{J}(w_k^i) > C})}{N_i} \\ &\approx \frac{P_i^{(2)}(1 - P_i^{(2)})}{N_i} \end{aligned} \quad (28)$$

Row 9 in Table 5 shows the variance of these conditional probability estimations.

When we neglect the small randomness in the estimated $\mathbb{P}(w \in S_i)$, the estimate of the unstart probability by Eq. (26) is unbiased. Because the samples in each stratum are independent, the variance of the estimator in Eq. (26) is

$$\text{Var}\left(\sum_{i=1}^3 \mathbb{P}(w \in S_i) \mathbb{P}(\mathcal{J}(w) > C | w \in S_i)\right) \quad (29)$$

From Table 5, we see that the stratified sampling algorithm has greatly reduced the variance compared with the naive Monte Carlo simulation with the same number of flow solutions as shown in Table 3. As can be seen in the table, the total variance of the stratified sampling is reduced to 31% that of the naive Monte Carlo method with 2100 flow solutions. The naive Monte Carlo method would need about 6600 samples in order to achieve the same level of variance. Because both the naive Monte Carlo method and our stratified sampling method produce unbiased estimators, the variance is synonymous with the mean square error. Therefore, the adjoint-based stratified sampling scheme is shown to accelerate the Monte Carlo method by a factor of more than three if the same level of error were desired.

IX. Optimal Allocation for Stratified Sampling

The efficiency of the adjoint-based stratified sampling scheme can be further improved by optimally allocating the number of flow solutions within each stratum. The optimal number of samples for each stratum can be calculated by solving the constrained optimization problem

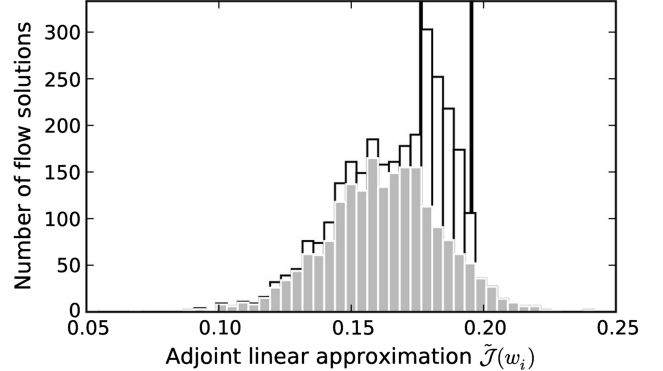


Fig. 13 Histogram of $\tilde{\mathcal{J}}$ for existing and additional flow solutions. Gray bars indicate existing flow solutions, and white bars on top of gray bars indicate additional flow solutions. The two vertical lines indicate the boundary between the three strata.

$$\min_{N_i} \text{Var}(P^{ss}) = \sum_{i=1}^3 \mathbb{P}(w \in S_i)^2 \frac{P_i^{(2)}(1 - P_i^{(2)})}{N_i} \quad \text{s.t. } \sum_{i=1}^3 N_i = N \quad (30)$$

Here, we minimize the total variance of the cost function, given that the total number of flow solutions is fixed. Using the Lagrange multiplier method, we take the derivative of the cost function and the constraint with respect to N_i and obtain the following relation:

$$\mathbb{P}(w \in S_i)^2 \frac{P_i^{(2)}(1 - P_i^{(2)})}{N_i^2} = \lambda \quad (31)$$

In other words, the optimal number of flow solutions in each domain should be proportional to

$$N_i \propto \mathbb{P}(w \in S_i) \sqrt{P_i^{(2)}(1 - P_i^{(2)})} \quad (32)$$

According to this formula, we calculated the optimal fraction of flow solutions in each stratum. The numbers are shown in row 3 of Table 6.

On top of the 2100 flow solutions that were performed in the last section, we now perform 900 additional flow solutions to further decrease the error in our estimation of the unstart probability. We allocate these additional flow solutions so that the total number of flow solutions in each stratum is as close as possible to the optimal fraction. The resulting number of additional flow calculations in each stratum is given in row 5 of Table 6. Figure 13 shows the histogram of the adjoint approximation $\tilde{\mathcal{J}}$ of the existing as well as the additional flow solutions. We can see from the table and the plot that most of the additional flow solutions are allocated in the uncertain stratum. This is because the uncertainty in this stratum, reflected by the variance of an individual sample $P_i^{(2)}(1 - P_i^{(2)})$, is highest.

Table 6 Summary statistics of optimal allocation for adjoint-based stratified sampling

	Stratus		
	Safe	Uncertain	Unstart
i	1	2	3
Optimal sample fraction based on Eq. (32)	0.6142	0.3766	0.0092
Existing number of flow solutions	1495	390	115
Additional flow solutions	231	669	0
Total flow solutions	1726	1059	115
Total number of unstart flow solutions	2	136	114
$P_i^{(2)} \approx \mathbb{P}(\mathcal{J}(w) > C w \in S_i)$	0.0012	0.128	0.9913
Estimator variance of $P_i^{(2)}$	6.7×10^{-7}	0.000106	0.000075
Contribution to the variance of P^{oa}	3.7×10^{-7}	4.03×10^{-6}	2.5×10^{-7}
$P^{oa} \approx \mathbb{P}(\mathcal{J}(w) > C)$		0.083	
Estimator variance of P^{oa}		4.65×10^{-6}	
2σ confidence interval of P^{oa}		(0.079, 0.087)	
Total number of flow solutions		3000	

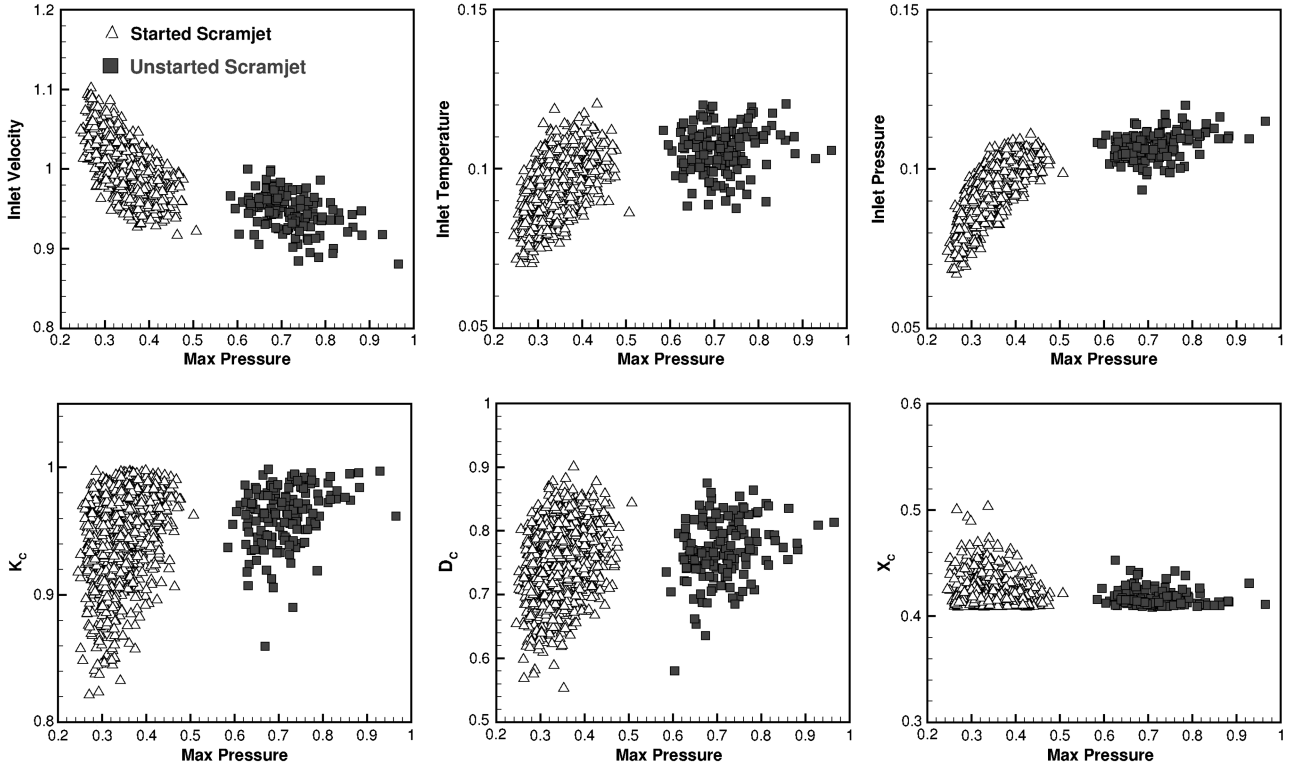


Fig. 14 Correlation plots of the maximum pressure in the combustor and each of the input variables. The two clusters correspond to started and unstarted solutions and confirm the clear distinction between the two scenarios.

Table 6 summarizes the computation of the unstart probability and its variance. By performing only 900 additional calculations, the variance, thus the mean square error, is reduced to 41% of that produced in the previous section. Compared with adding the same number of flow solutions but with the same suboptimal allocation strategy, the optimal allocation strategy further accelerated the Monte Carlo sampling method by 67%. With the naive Monte Carlo method with 3000 flow solutions, the adjoint-based stratified

sampling algorithm with optimal allocation reduces the variance (thus mean square error) to 18.6% that of naive Monte Carlo. In other words, it accelerated Monte Carlo sampling by a factor of 5.4.

X. Analysis of the Unstart Simulations

The quantification of the probability of unstart is only the first step toward assessing the reliability of the propulsion system; the

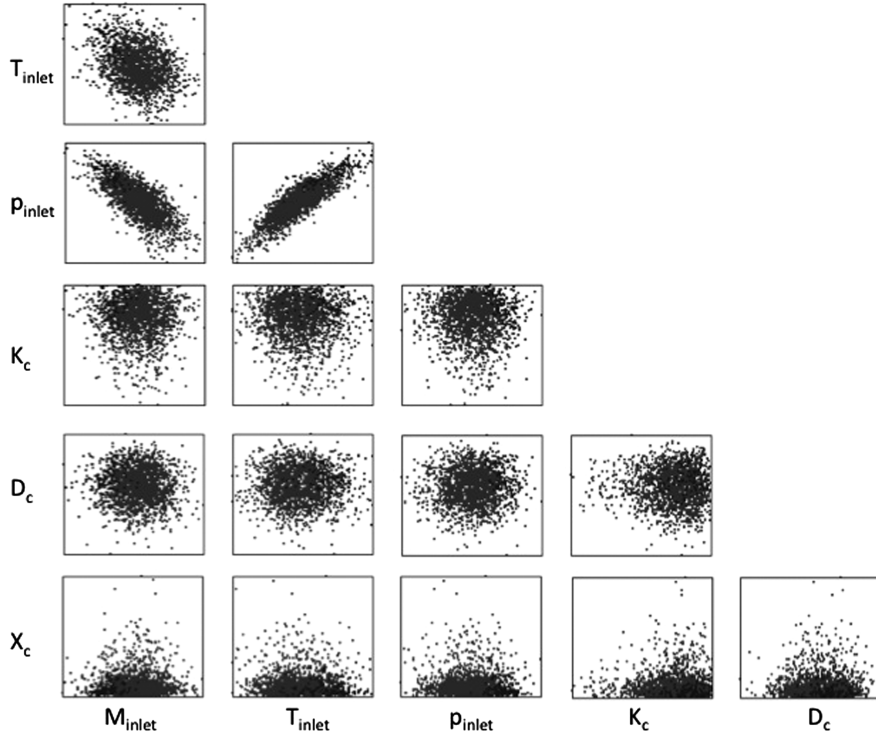


Fig. 15 Cross-correlation plots of the uncertain inputs.

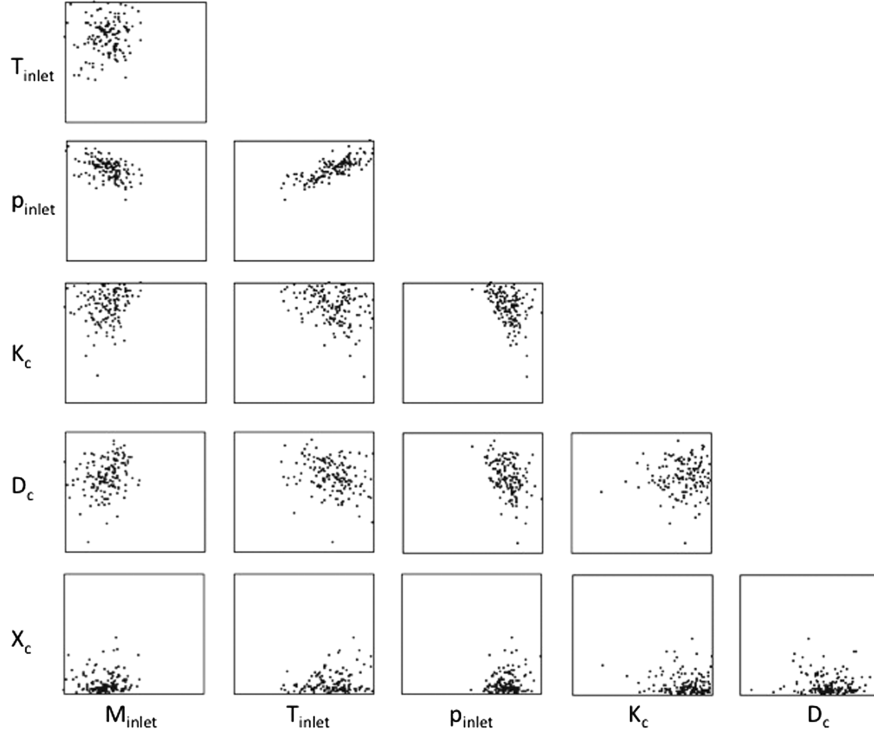


Fig. 16 Cross-correlation plots of the uncertain inputs conditioned on the unstart occurrence.

characterization of the operability limits in terms of correlations between the input uncertainties and the system failure can lead to improved design and a better understanding of the physics of unstart.

In this section, we report a brief analysis that illustrates how the system behaves in the neighborhood of the operability limit. A detailed analysis is beyond the scope of the present paper as the input uncertainties are artificially introduced and do not correspond precisely to the operating scenario of the HyShot II vehicle.

As a first step, we study the correlation of the input quantities with the maximum pressure in the combustor, which has been used previously as a means to detect unstart (Fig. 14). Two important observations can be made by plotting the results for all the Monte Carlo realizations; the first is that two clusters of solutions are clearly identified. The first corresponds to lower values of the pressure and to started combustors. This confirms the analysis of the probability distribution function reported in Fig. 8 and the definition of the critical pressure. A second interesting result is that the maximum pressure is well correlated with the input parameters (for example, inlet pressure) only for the started cases. A relatively large scatter is present for the unstarted cases. This seems to indicate that the actual maximum pressure attained during an unstart event is potentially a very complex function of multiple variables, and the operability bound is sharp.

An alternative characterization of the system is based on cross correlations between the input parameters as reported in Fig. 15. In this case, the only clear trend is the presence of a correlation between inlet pressure and Mach number that can be explained with the generation of the combustor inlet conditions starting from the uncertainty in the flight environment as illustrated before. In Fig. 15, all the realizations are reported; on the other hand, in Fig. 16, the correlations are conditioned on the presence of unstart. The ranges of the input variables are the same as in Fig. 15, but it is clear that there exist regions in which unstart does not occur. For example, if the heat is released toward the exit of the combustor (large x_c), then thermal choking will not occur. Another expected result is that unstart is more likely if the incoming stream is at a lower Mach number. The effect of the uncertain parameters in the combustion model, especially D_c , proves more difficult, as no clear trend emerges; specifically, it appears that unstart can occur independently of the value of D_c , which represents the shape factor for the heat release. Similarly, there is only a vague trend for the amount of fuel burnt, parameterized by

K_c ; although obviously high values of K_c are more likely to lead to thermal choking, few unstarted realizations with $K_c < 0.85$ were observed.

Using adjoint-computed gradient information at multiple locations in the parameter space [25,26] could improve the accuracy of the adjoint linear approximation, thereby further enhance the efficiency of this method. These locations could include parameter combinations that lead to unstart. We plan to solve the unsteady adjoint equations [27,28] for computing the derivatives at unstart conditions. Such an approach will be investigated in future work.

XI. Conclusions

This study demonstrates an adjoint-based approach for accelerating Monte Carlo estimations of risk. The approach is applied to estimating the unstart probability of a scramjet engine under uncertain operating conditions. The uncertainty is described by five random input parameters with various Gaussian and non-Gaussian distributions. Unstart can be identified by the existence of a strong normal shock wave in the combustor, creating a large pressure peak on the combustor wall. In this study, the objective function \mathcal{J} is defined as the eighth norm of the upper combustor wall pressure and unstart is quantitatively determined as the objective function exceeding a certain critical value.

The adjoint equation was solved with respect to the objective function \mathcal{J} , and the adjoint solution was used to generate a linear approximation to the objective function. Because of the strong nonlinearities in the problem, the linear approximation can be inaccurate in regions of the parameter space that are distant from the linearized state. Nevertheless, this adjoint linear approximation is computationally inexpensive to evaluate and correlates well with the true value of the objective function. These two characteristics enable variance reduction of the Monte Carlo approach based on the linear approximation.

Adjoint-based stratified sampling has been applied to reduce the variance of our estimate of the unstart probability. The sample space of the uncertain input parameters is divided into three different strata (corresponding to safe operation of the engine, uncertain operation, and unstart) based on the adjoint linear approximation. The probability of unstart within these strata is very different and, as a result, stratified sampling based on these strata significantly reduces

the variance, thus the mean square error of the estimator. The optimal fraction of flow calculations within each stratum was further calculated. Stratified sampling with optimal allocation of samples further reduces the variance of the estimator. Using the adjoint-based variance reduction technique, the Monte Carlo method was demonstrated to be accelerated by a factor of 5.4. Although an exhaustive study of the input/output correlations that induce thermal choking is beyond the scope of this paper, a brief analysis has been reported to show how the operability limits can be mapped in terms of input variability.

Acknowledgments

This material is based upon work supported by the Department of Energy (National Nuclear Security Administration) under award number NA28614. This report was prepared as an account of work sponsored by an agency of the U.S. Government. Neither the U.S. Government nor any agency thereof, nor any of their employees makes any warranty, express or implied, or assumes any legal liability or responsibility for the accuracy, completeness, or usefulness of any information, apparatus, product, or process disclosed, or represents that its use would not infringe privately owned rights. Reference herein to any specific commercial product, process, or service by trade name, trademark, manufacturer, or otherwise does not necessarily constitute or imply its endorsement, recommendation, or favoring by the U.S. Government or any agency thereof. The views and opinions of the authors expressed herein do not necessarily state or reflect those of the U.S. Government or any agency thereof.

Reference

- [1] Rausch, V., McClinton, C., Sitz, J., and Reukauf, P., "NASA's Hyper-X Program," NASA Dryden Flight Research Center Document No. 20010075170, 2009.
- [2] Hank, J., Murphy, J., and Mutzman, R., "The X51-A Scramjet Engine Flight Demonstration Program," 15th AIAA International Space Planes and Hypersonic Systems and Technologies Conference, AIAA Paper 2008-2540, 2008.
- [3] Auslender, A., Suder, K., and Thomas, S., "An Overview of the NASA FAP Hypersonics Project Airbreathing Propulsion Research," 16th AIAA/DLR/DGLR International Space Planes and Hypersonic Systems and Technologies Conference, AIAA Paper 2009-7277, 2009.
- [4] Mayer, D., and Paynter, G., "Prediction of Supersonic Inlet Unstart Caused by Freestream Disturbances," AIAA Paper 1994-0580, 1994.
- [5] Star, J., Edwards, J., Smart, M. K., and Baurle, R., "Investigation of Scramjet Flow Path Instability in a Shock Tunnel," AIAA Paper 2006-3040, 2006.
- [6] Pecnik, R., Terrapon, V., Ham, F., and Iaccarino, G., "Full System Scramjet Simulation," Annual Research Briefs, Center for Turbulence Research, Stanford, CA, 2009, pp. 33–45.
- [7] Smart, M., Hass, N., and Paull, A., "Flight Data Analysis of the HyShot 2 Scramjet Flight Experiment," AIAA Journal, Vol. 44, 2006, pp. 2366–2375.
doi:10.2514/1.20661
- [8] Schramm, J., Karl, S., Hanneman, K., and Steelant, J., "Ground Testing of the HyShot II Scramjet Configuration in HEG," AIAA Paper 2008-2547, 2008.
- [9] Liepmann, H. W., and Roshko, A., *Elements of Gas Dynamics*, Wiley, New York, 1957, Chap. 4.
- [10] Doolan, C., and Boyce, R., "A Quasi-One-Dimensional Mixing and Combustion Code for Trajectory Optimisation and Design Studies," AIAA Paper 2008-2603, 2008.
- [11] Jameson, A., "Aerodynamic Design via Control Theory," *Journal of Scientific Computing*, Vol. 3, 1988, pp. 233–260.
- [12] Giles, M., and Pierce, N., "Adjoint Equations in CFD: Duality, Boundary Conditions and Solution Behaviour," AIAA Paper 1997-1850, 1997.
- [13] Giles, M., Duta, M., Müller, J., and Pierce, N., "Algorithm Developments for Discrete Adjoint Methods," *AIAA Journal*, Vol. 41, 2003, pp. 198–205.
doi:10.2514/2.1961
- [14] Pecnik, R., Terrapon, V., Ham, F., and Iaccarino, G., "Full-System RANS of the HyShot II Scramjet Part 1: Numerics and Non-Reactive Simulations," *Annual Research Briefs, Center for Turbulence Research*, Stanford Univ., Stanford, CA, 2010, pp. 57–68.
- [15] Emory, M., Terrapon, V., Pecnik, R., and Iaccarino, G., "Characterizing the Operability Limits of the HyShot II Scramjet Through RANS Simulations," AIAA Paper 2011-2282, 2011.
- [16] Griewank, A., Juedes, D., and Utke, J., "Algorithm 755: ADOL-C: A Package for the Automatic Differentiation of Algorithms Written in C/C++," *ACM Transactions on Mathematical Software*, Vol. 22, 1996, pp. 131–167.
doi:10.1145/229473.229474
- [17] Griewank, A., "A Mathematical View of Automatic Differentiation," *Acta Numerica*, Vol. 12, 2003, pp. 321–398.
doi:10.1017/S0962492902000132
- [18] Lien, J., Bose, D., and Martin, J., "Automated Sensitivity Analysis of Hyper-X (X-43A) Separation Simulation," AIAA Paper 2004-4930, 2004.
- [19] Baumann, E., Beck, R., and Richard, M., "The X-43A Six-Degree of Freedom Monte Carlo Analysis," AIAA Paper 2008-0203, 2008.
- [20] Huebner, L., Rock, K., Ruf, E., Witte, D., and Andrews, E. H., "Hyper-X Flight Engine Ground Testing for X-43 Flight Risk Reduction," AIAA Paper 2001-2803, 2001.
- [21] Trucano, T. G., "Prediction and Uncertainty in Computational Modeling of Complex Phenomena: A Whitepaper," Sandia National Labs. Rept. 98-2776, Albuquerque, NM, 1998.
- [22] Iaccarino, G., Pecnik, R., Glimm, J., and Sharp, D., "A QMU Approach for Characterizing the Operability Limits of Air-Breathing Hypersonic Vehicles," *Reliability Engineering and System Safety*, Vol. 96, No. 9, 2010, pp. 1150–1160.
doi:10.1016/j.ress.2010.06.030
- [23] Giunta, A., Eldred, M., Swiler, L., Trucano, T., and Wojtkiewicz, S., "Perspective on Optimization Under Uncertainty: Algorithms and Applications," AIAA Paper 2004-4451, 2004.
- [24] Wang, Q., "Uncertainty Quantification for Unsteady Fluid Flow Using Adjoint-based Approaches," Ph.D. Thesis, Stanford Univ., Stanford, CA, 2009.
- [25] Wang, Q., Moin, P., and Iaccarino, G., "A Rational Interpolation Scheme with Super-Polynomial Rate of Convergence," *SIAM Journal on Numerical Analysis*, Vol. 47, No. 6, 2010, pp. 4073–4097.
doi:10.1137/080741574
- [26] Wang, Q., Moin, P., and Iaccarino, G., "A High Order Multivariate Approximation Scheme for Scattered Data Sets," *Journal of Computational Physics*, Vol. 229, No. 18, 2010, pp. 6343–6361.
doi:10.1016/j.jcp.2010.04.047
- [27] Wang, Q., Moin, P., and Iaccarino, G., "Minimal Repetition Dynamic Checkpointing Algorithm for Unsteady Adjoint Calculation," *SIAM Journal on Scientific Computing*, Vol. 31, No. 4, 2009, pp. 2549–2567.
doi:10.1137/080727890
- [28] Wang, Q., Gleich, D., Saberi, A., Etemadi, N., and Moin, P., "A Monte Carlo Method for Solving Unsteady Adjoint Equations," *Journal of Computational Physics*, Vol. 227, No. 12, June 2008, pp. 6184–6205.
doi:10.1016/j.jcp.2008.03.006

F. Ladeinde
Associate Editor